mCCDcl1 cells show Plasticity Consistent with the Ability to Transition between Principal and Intercalated Cells

$mCCD_{cl1}$ cells show Plasticity Consistent with the Ability to Transition between Principal and Intercalated Cells

A.M. Assmus, M.K. Mansley, L.J. Mullins, A. Peter, J.J. Mullins

University of Edinburgh/BHF Centre for Cardiovascular Science, The University of Edinburgh, Edinburgh, UK EH16 4TJ

Running title:

Plasticity of $mCCD_{cl1}$ cells

Corresponding author:

Adrienne Assmus

Centre for Cardiovascular Science,

Queen's Medical Research Institute,

47, Little France Crescent

Edinburgh, EH16 4TJ, UK

s1373589@ed.ac.uk

Abstract

The cortical collecting duct of the mammalian kidney plays a critical role in the regulation of body volume, sodium pH and osmolarity and is composed of two distinct cells types, principal cells and intercalated cells. Each cell type is detectable in the kidney by the localization of specific transport proteins such as Aqp2 and ENaC in principal cells and V-ATPase B1 and Cx30 in intercalated cells. $mCCD_{cl1}$ cells have been widely used as a mouse principal cell line on the basis of their physiological characteristics. In this study, the $mCCD_{cl1}$ parental cell line and three sub-lines cloned from isolated single cells (Ed1, Ed2, and Ed3) were grown on filters to assess their transepithelial resistance, transepithelial voltage, equivalent short circuit current and expression of the cell-specific markers Aqp2, ENaC, V-ATPaseB1 and Cx30. The parental $mCCD_{cl1}$ cell line presented amiloride-sensitive electrogenic sodium transport indicative of principal cell function, however immunocytochemistry and RT-PCR showed that some cells expressed the intercalated cell-specific markers V-ATPase B1 and Cx30, including a subset of cells also positive for Aqp2 and ENaC. The three subclonal lines contained cells that were positive for both intercalated and principal cell-specific markers. The vertical transmission of both principal and intercalated cell characteristics via single cell cloning, reveals the plasticity of $mCCD_{cl1}$ cells, and a direct lineage relationship between these two physiologically important cell types, and is consistent with $mCCD_{cl1}$ cells being precursor cells.

Introduction

The collecting duct of the mammalian kidney is responsible for 4-5% of total sodium reabsorption and approximately 10% of total water reabsorption from the ultrafiltrate. It plays a critical role in the regulation of urine volume, pH and osmolarity, with two thirds of the hypo-osmotic fluid entering the collecting duct being reabsorbed in the CCD (cortical collecting duct) (10).

The CCD is composed of two distinct cells types, principal cells (PCs) and intercalated cells (ICs), the latter being sub-divided into α and β subtypes. Principal and intercalated cells can be distinguished by morphological and immunocytochemical criteria and are functionally specialized. Principal cells reabsorb water and sodium through aquaporin2 (Aqp2) and the epithelial sodium channel (ENaC) respectively, are responsible for K^+ excretion and express several physiologically important genes including *Hsd11b2*. In contrast, intercalated cells regulate urinary pH through V-ATPase, reabsorb K^+ through H^+/K^+ATPase and produce ATP via the Connexin 30 (Cx30) apical membrane hemichannels (33). The different cell types are detectable in the kidney by immunostaining. Typically, PCs show apical membrane staining for Aqp2 or ENaC channels. V-ATPase localises to the apical membrane of α-ICs, and the Cl^-/HCO_3^- exchanger

AE1 localises to the basolateral membrane. Conversely V-ATPase localises to the basolateral membrane in β-ICs.. Morphological differences include the presence of a primary central cilium on PCs while the apical membrane of ICs are covered with a dense layer of microvilli (27).

In the mouse CCD, the ratio between PCs and ICs is approximately 70:30 (14), but the lineage relationship between these cells is unclear. Although PCs and ICs appear distinct, they exhibit a degree of functional overlaps and inter-regulation. For example, sodium reabsorption can occur through thiazide-sensitive transport in β-IC (20) in addition to reabsorption through ENaC in PCs. Furthermore, ATP released from Cx30 in ICs is an inhibitory regulator of sodium and water reabsorption via calcium signaling, resulting in sodium regulation in PCs (22). Sodium, water, and potassium transport in PCs are also regulated through the paracrine ATP/prostaglandin E2 (ATP/PGE2) signaling cascade involving ICs (13). ICs also appear to have plasticity between α- and β-ICs under acidotic conditions or the deletion of the extracellular matrix protein DMBT1 (1, 12), as well as the existence of a third IC type in the collecting duct characterized by the presence of apical V-ATPase but no bicarbonate exchanger AE1 on the basolateral membrane (17).

The ratio of principal cells to intercalated cells is influenced by multiple factors including the transcription factor Adam10 and the E3 ubiquitin ligase Mib1, both of which are required for Notch signaling, and the histone H3 K79 methyltransferase Dot1l. The deletion of floxed alleles of *Adam 10*, *Mib1* and *Dot1l* via genetic crosses with *Aqp2-cre* (for Adam10$^{f/f}$) or *Hoxb7-cre* (for Dot1l$^{f/f}$ and Mib1$^{f/f}$) mice, results in a reduced number of principal cells (14, 15, 38). Whilst it is evident that activation of the Notch pathway is important in determining CCD identity, the underlying mechanisms remain unclear. Studies of the *Dot1l*$^{-/-}$ mice also showed that ICs lacked di-methyl K79 suggesting that the cells had previously expressed Aqp2-cre and therefore presumed to be *Dot1l*$^{-/-}$ and originate from PC cells (37). Earlier studies on primary mouse β-ICs showed they can give rise to both α-ICs and PCs, however cultures of primary PCs did not appear to show the same capacity for interconversion (8). Related studies on immortalized M1 cells showed a proportion of cells expressing a dual phenotype suggesting a degree of cell plasticity and *in vivo* evidence for bi-potential comes from studies of *Foxi1*$^{-/-}$ mice in which the collecting ducts comprised of a single cell type that was positive for both principal and intercalated cell markers (37). Finally, it has recently been reported that a subset of ureteric bud tip cells (UBTCs) expressing p63 act as progenitors for cortical intercalated cells and that cell determination, at least for this population of IC cells, may already be specified at this early stage of development (7). The inter-relationship between PC and IC cells, both during development and in the adult, is complex and is yet to be fully elucidated.

mCCD$_{cl1}$ cells have been described as a spontaneously transformed cell line derived from a single clone,

which was obtained by microdissecting the cortical collecting duct of a wild type mouse (11). $mCCD_{cl1}$ cells express ENaC as well as the necessary cellular machinery, including 11 beta-hydroxysteroid dehydrogenase type 2 (HSD11b2), mineralocorticoid and glucocorticoid receptors (MR and GR), to enable their stimulation by physiological concentrations of aldosterone and have therefore been used as a model for studying PC physiology. The $mCCD_{cl1}$ cells have proved to be a useful tool for studying the regulation of principal cell ion transporters such as ENaC (4, 30) or ROMK channels (9). In these studies, $mCCD_{cl1}$ cells have been shown to possess the functions of *in vivo* CCDs, and are therefore considered to be a "highly differentiated murine principal cell line" (21). However, here we show that $mCCD_{cl1}$ is a heterogenous cell population expressing PC and IC markers Precursor cells expressing both PC and IC markers are reminiscent of dual-staining transition cells, recently observed *in vivo* in the collecting duct (36). Moreover, we used clonal cell sublines to show that this heterogeneity could be transmitted through a single cell and that $mCCD_{cl1}$ cells exhibit a renewable bi-potential phenotypic characteristic of precursor cells.

Methods

Cell culture

The $mCCD_{cl1}$ cell line was previously established and kindly provided by Bernard Rossier (University of Lausanne, Lausanne, Switzerland). The cells were cultured at 37°C and 5% CO_2 in Phenol red free DMEM/F12 media (Invitrogen, Life Technologies), with the following supplements: insulin (5µg/ml), triiodothyronine (1nmol/l), sodium selenite (60nmol/l), dexamethasone (50nmol/l), apotransferrin (5µg/ml), EGF (10ng/ml), FBS (2%), and penicillin-streptomycin (Pen-Strep, 100U/ml-100µg/ml) for optimal culture conditions as previously described (11).

Cloning

Clonal cell lines derived from $mCCD_{cl1}$ cells were established using the dilution method as previously described (28). Briefly, confluent $mCCD_{cl1}$ cells in growth medium were trypsinized, suspended in medium, and serially diluted in a 96-well plate. Following appropriate dilution, the presence of single cells was independently verified and confirmed by observing the growth of the resulting single colonies in the wells over 3 days of culture. The colonies were then trypsinized and transferred to a T75 flask for culture. The cloning process produced 8 clonal sub-lines, among which 3 lines (named Ed1, Ed2 and Ed3) were selected for further studies based on morphological differences.

Polarization and TEER Measurements

Parental $mCCD_{cl1}$ cells were used between passages 26 and 30. Parental cells and clonal sub-lines were polarized by growing cells on Corning Costar™ Snapwell™ Permeable Supports inserts (12mm, 0.4 μm pore size). Cells were seeded at a 1:1 split ratio and grown for 10 days. On day 8, the cells were fed with basal medium containing charcoal-stripped FBS and Pen-Strep supplements only and on day 9 with basal media containing Pen-Strep only. Measurements for transepithelial voltage (V_{te}) and transepithelial resistance (R_{te}) were made with a transepithelial volt-ohm-meter and a set of chopstick "STX" electrodes ($EVOM^2$, World Precision Instruments) and the equivalent short circuit current (I_{sc}) calculated using Ohm's law. By convention, a negative Isc reflects either electrogenic secretion of cations, electrogenic absorption of anions, or a combination of both. Aldosterone and amiloride (Sigma Life Science, UK) were used at 3nM and 10μM respectively.

Immunocytochemistry

Immunocytochemistry was performed on cells cultured on the Snapwell™ permeable membranes as described previously. Cells were fixed using 4% PFA for 20min. Double immunostaining of Aqp2 and Cx30 was made using polyclonal goat anti-mouse Aqp2 (Abcam ab105171; 1:200) and rabbit anti-mouse Cx30 antibody (Invitrogen 712200; 1:100). The fluorescent secondary antibodies were Alexa Fluor 568- and 488- donkey anti-rabbit and anti-goat respectively, at a dilution of 1:500. Immunostaining for ENaC and V-ATPase was conducted using a rabbit anti-mouse α-ENaC antibody (1:1000; kindly provided by Prof. J. Loffing, University of Zurich, Switzerland) and a goat anti-mouse V-ATPase A1 antibody (Santa Cruz Biotechnology, sc-28801; 1:50), with the fluorescent secondary antibodies described above. Immunostaining for V-ATPase B1 was performed with a rabbit anti-mouse antibody (Life Technologies, PA535052, 1:50), conjugated to Alexa Fluor 568. Triple immunocytochemistry was performed on the parental $mCCD_{cl1}$ cell line with the same primary antibodies for V-ATPase and α-ENaC, and the addition of an anti-acetylated α-tubulin conjugated antibody at a dilution of 1:50 (Santa-Cruz Technologies, sc-

23950 with AF488, green secondary). Alexa Fluor 647 (far red) was used as the fluorescent secondary antibodies for V-ATPase in this experiment. Immunocytochemistry for p63 and ΔNp63 was performed using a rabbit anti-mouse ΔNp3 antibody and a goat anti-mouse p63 antibody (Biolegend 619001, 1:500, and abcam ab114059, 1:200, respectively).

The permeable membranes were cut from their support using a scalpel blade, and mounted on microscope slides with DAPI mounting medium (Prolong Gold antifade reagent with DAPI, Life Technologies). Images were taken with a Q-Imaging camera (Canada) on a Nikon Eclipe Ti fluorescent microscope, with DAPI, FITC, TRITC, and CY5 filters applied, for DAPI, Alexa fluor 568, 488, and 647 respectively. Both 60X 1.4 NA Plan Apo and 40X 1.3 NA Plan Flur oil objectives were used. To visualize cell polarization, cells were imaged using an Andor Revolution spinning disc microscope (Oxford Instruments), with the iQ3 imaging software and the iXon EMCCD camera. The 40x 1.3NA (oil immersion) objective was used. Excitation was performed at 569nm, for detection of Alexa Fluor 594 fluorophore (conjugated to the α-ENaC antibody). Cell autofluorescence was imaged with excitation at 405nm.

RT-PCR and RNA Sequencing

Total RNA was extracted from $mCCD_{cl1}$ cells and the clonal cell lines Ed1, Ed2 and Ed3 using TRIzol (Ambion, Life Technologies). The concentration, purity and integrity of the RNA obtained were verified using the 260-to-280-nm optical density ratio on a NanoDrop, and by running the RNA on a 1% agarose gel to visualize ribosomal RNA 28S and 18S bands. cDNA was obtained using 500ng of RNA with a High capacity RNA-to-cDNA Kit (Applied Biosystems). The primer sequences for each transcript were obtained using PrimerBank (Table 1). The reactions were carried out in a Veriti 96-well Thermal Cycler (Applied Bioscience) and the amplified PCR products separated by electrophoresis in a 2% agarose gel.

For RNA sequencing, $mCCD_{cl1}$, Ed1, Ed2 and Ed3 cells were cultured in T75 flasks for one week then each line was passaged in three T25 flasks and cultured for one week before using Trizol to extract the RNA. RNA was purified from genomic DNA using DNase Kit RNeasy Plus (Qiagen, USA). The process gave 12 samples comprising of three replicates of each cell line. RNA purity and concentration were determined as described above. Stranded total RNA libraries were prepared (Source Bioscience Plc (Nottingham, UK)) according to the Illumina TruSeq Stranded mRNA sample preparation protocol and validated on the Agilant BioAnalyser 2100. Illumina Paired-End multiplexed sequencing was undertaken using the Illumina NextSeq sequencing platform. Read quality was checked using FastQC (2) and reads were trimmed with Trimmomatic (3) yielding 20-58 million read pairs per sample. Reads were aligned with HISAT2 (16) to the Ensembl mouse GRCm38 genome (mm10). Strandedness and read distribution was assessed using RSeQC (35) and quasi-alignment using Salmon (24) for transcript quantification.

Estimated counts were adjusted for library size and transcript length using tximport (31). Matices were filtered and normalised using the trimmed Mean of M values method (26) and differential expression was carried out using edgeR version 3.12.0 (25).

Data analysis

Data were analyzed using GraphPad Prism 7.0 (GraphPad Software) and statistical significance was assessed using a Student paired t-test or one way ANOVA where appropriate. Data are expressed as mean ± SD, and *n* values refers to the number of repeats in an experiment. For each repeat, experimental conditions were matched as closely as possible.

Image analysis

All the images were analyzed using ImageJ software (National Institutes of Health). Data were obtained by measuring the mean grey value of the cell surfaces. The mean grey value corresponds to the mean brightness level of the selected surface, and it was measured in 50 immuno-positive cells for each cell passage (n=4) in the appropriate color channels, for a total of 200 immuno-positive cells per cell line. The grey values attributed to background auto-fluorescence on the different channels were measured on a control area (no cells) and subtracted from the grey values of the cells.

Results

$mCCD_{cl1}$ cells possess the functional characteristics of PCs but also express IC-related markers.

Transepithelial electrophysiological measurements of parental $mCCD_{cl1}$ cells revealed baseline I_{sc} measurements of -9.0 ± 1.0μA/cm^2 (n=4), consistent with previous reports (11, 21). The application of amiloride (10μM, 10 min) to the apical bath inhibited I_{sc} by 82.1 ± 8.2%, indicating that the basal current can mostly, but not totally, be attributed to the transport of Na^+ via ENaC. The addition of aldosterone (3nM, 3 h) increased I_{sc} by a factor of 3.8 ± 0.2 fold, to reach values of -34.0 ± 1.2 μA/cm^2. I_{sc}, R_{te} and V_{te} values are shown in Table 2. Cell polarization was observed using confocal microscopy on $mCCD_{cl1}$ stained with an anti-α-ENaC antibody (Figure 1e).

For characterization of the cell line, immunocytochemistry double-labelling analyses were performed on $mCCD_{cl1}$ cells using antibodies against Aqp2 and Cx30, Aqp2 and V-ATPase B1 (Figure 1a and 1b). or α-ENaC and V-ATPase A1 (Figure 1c). The cells expressed the expected PC markers Aqp2 (green) and α-ENaC (red). Unexpectedly, numerous cells also expressed the typical IC markers V-ATPase B1 and Cx30 (Figure 1a and 1b). At higher magnification, the localisation of Cx30 and Aqp2 staining in $mCCD_{cl1}$

cells shows that while some cells only stain for PC or IC markers, many cells express markers of both cells, suggesting an "intermediate" or transition cell type (Figure 1d). A similar phenotype was observed with cells stained for V-ATPase B1 and Aqp2. Whilst 47% of total cells did not show any significant staining, 42% of cells stained for both markers (dual-character/bi-potential), while cells staining for only Aqp2 represented ~9% and cells with V-ATPase ~2%.

Immunocytochemistry using an anti-acetylated α-tubulin antibody showed that very few cells staining positive for α-ENaC displayed primary cilia, and in those that did the cilia appeared short (Figure 2c). The anti-acetylated α-tubulin antibody also stains the intracellular acetylated micro-tubular cytoskeleton, considered more stable than its non-acetylated counterpart. Cells displaying strong V-ATPase A1 staining showed a lack of staining for acetylated α-tubulin (Figure 2a). This observation was confirmed by the quantification of mean grey value for both markers in 60 immuno-positive cells displaying a range of different V-ATPase A1 staining intensities, with mean grey values < 5% considered low, and >5% considered high. A paired t-test applied to both populations (high or low V-ATPase A1) showed a significant difference between the mean fluorescence intensities of V-ATPase A1 and acetylated α-tubulin, and an inverse correlation between these two markers (Figure 2b). These data suggest that an acetylated alpha-tubulin-positive cytoskeleton could be used as an additional marker for PCs as well as cells possessing both PC and IC characteristics. The immunocytochemistry data led to the description of four groups of cells, PC^+/IC^-, PC^-/IC^+, PC^+/IC^+, and PC^-/IC^- the characteristics of which are summarized in Table 3.

The bi-potential PC-IC cell phenotype is transmitted through a single $mCCD_{cl1}$ cell to clonal cell lines.

Dilution cloning of the $mCCD_{cl1}$ (parental) cell line produced 8 clonal sublines derived from single cells, among which the exemplary Ed1, Ed2 and Ed3 were selected for further studies based on their morphology displayed at confluency, in particular their different average cell size. RT-PCR of Aqp2 and Cx30 (Figure 3c) showed expression of both PC and IC markers in all three sublines. Immunocytochemistry of V-ATPase B1 and Aqp2 (Figure 3a) in the three sublines showed the presence of PC^+/IC^+ characteristics, as described above for the parental line. These PC^+/IC^+ cells are detectable in different proportions when comparing each clone and the parental line (Figure 3b). PC^+/IC^+ cells comprised 24.1 ± 7.1 % of Ed1, 32.8 ± 7.2 % of Ed2 and 45.5 ± 5.7 % of Ed3 respectively. PC^-/IC^+ cells were most represented in Ed2 with 5.7 ± 1.9 %. Ed3 is the closest to the parental line, with PC^+/IC^+ cells representing 45.5 ± 5.7% of the total. In the parental and clonal sublines, the PC^+/IC^+ group makes up more than 50% of the cells showing significant staining, showing that the capacity for the cells to possess both IC and PC characteristics can be transmitted through a single cell of the $mCCD_{cl1}$ parental line.

The data from the α-ENaC staining (Figure 3d and 3e) can be compared with the electrophysiological measurements performed on the clonal sublines (Figure 4a-d and Table 2). Basal currents in Ed1 and Ed3 were 81.8 ± 7.0 and 88.4 ± 3.1% amiloride sensitive, respectively, indicating that, similar to the parental line, their basal currents can principally be attributed to the transport of Na^+ via ENaC. Baseline I_{sc} in Ed2, showed significantly lower ENaC expression levels (mean grey value at 2.0 ± 0.4 % vs 7.2 ± 0.9 % respectively) was negligible compared to the parental line (-1.4 ± 0.4 μA/cm^2 v -9.0 ± 1.0 μA/cm^2, respectively). Ed1, consisting of ~90% of dual-staining cells, did not develop a cell layer as resistive as the parental line, with a maximum R_{te} at day 10 of 0.8 ± 0.1 kΩ·cm^2. V_{te} of Ed1 cells also remained lower than for the parental line throughout the experiments, reaching a maximum of -18.1 ± 0.5 mV on day 8, compared to V_{te} of parental cells at day 8 of -32.7 ± 1.0 mV. These electrophysiological measurements for Ed1 reflect the ENaC expression level, which at 3.5 ± 0.4 % sits between Ed2 and $mCCD_{cl1}$. Ed3 was closer to the parental line in terms of ENaC immunostaining levels (mean grey value at 7.1 ± 0.6 %), and developed strong R_{te} and V_{te}, significantly greater than the parental line. Baseline I_{sc} for $mCCD_{cl1}$, Ed1 and Ed3 were similar, but the aldosterone responses of the sub-lines were significantly lower than the parental line, with I_{sc} fold changes for baseline-to-aldosterone treatment at 3.8 ± 0.3 for the parental line, and 2.1 ± 0.2 for Ed1 and Ed3 (Table 2). The responses to aldosterone and amiloride for Ed2 were considered not relevant due to the negligible baseline I_{sc}. Electrophysiological measurements made from clonal sublines and the parental line remained consistent throughout experiments (n=4), suggesting that at a cell population level, the cells exhibit a stable phenotype.

RNA Sequencing confirms important differences between parental line and sublines, and also expression of IC-specific proteins.

RNASeq was performed on RNA obtained from parental $mCCD_{cl1}$ cells and the Ed1, Ed2, and Ed3 (n=3).

Visualization of the data by principal component analysis shows the differences between the clonal lines and the parental line. The first three principal components (PC1-3) represent 90% of the total variability observed in the dataset (Figure 5a). PC1 corresponds to 59.8% of total variability, PC2 18.3% and PC3 11.9%. Whilst the repeats are grouped together, indicating the stability of expression between different samples of the same cell line, the projection of the data on the three main principal components axis shows heterogeneity of expression between the parental $mCCD_{cl1}$ cells and the three sublines. These differences are easily visualized using a clustering dendrogram (Figure 5b), showing the variance between the four cells lines by using the top 1000 genes with the most important variability between samples. The extent of the difference between $mCCD_{cl1}$ and the three sublines can be interpreted by looking at the height of the bars linking each sample. The data show that whilst the transcriptome was reproducible between repeats, it differed significantly between the four lines and that Ed3 and Ed1 showed the greatest

similarity and difference, respectively, with $mCCD_{cl1}$. The top twenty transcripts showing the widest differential expression between parental and clonal cell lines, highlighting the heterogenous nature of the $mCCD_{cl1}$ cell line are shown in Table 4.

As predicted from the immunocytochemistry data, the expression of genes associated with differentiated ICs and PCs varied between the individual clones. Expression of the α-IC-specific sodium potassium chloride co-transporter NKCC1 (SLC12A2), β-IC specific genes such as the sodium bicarbonate exchanger NDCBE-3 (SLC4A8), the ATPase H+ transporter (Atp6v1b1), the potassium chloride co-transporter KCC (SLC12A5) and the chloride channel ClCK2 (CLCNKB), and the α/β-IC-specific sulphate transporter SLC26A11 were observed in the parental cell line and all three sub-clones. PC-specific genes such as the renal outer medullary potassium channel ROMK (Kcnj1), Kir4.1 (Kcnj10), 11βHSD2 (HSD11B2), aquaporin 4 (AQP4), and sodium-potassium ATPase (ATP1A1) were also detected in all four cell lines (Table 4 and data not shown).

The RNA-Seq data also reveals expression of a number of progenitor cell markers, including Pax2, p63, CD24, CD133, Sca-1, and NfatC1, the latter previously ascribed to apoptosis-resistant renal progenitor cells (19). The expression of specific collecting duct precursor cell markers in the RNA-Seq was confirmed by staining the parental $mCCD_{cl1}$ cells and the clonal lines for p63, which has been observed in the ureteric bud, and ΔNp63 (7). All the cell lines show significant staining for both markers (Fig. 6a), but with variable sub-cellular localization: p63 was either localized around the nucleus or, infrequently, more widely throughout the cell. The p63 marker was found to co-localise with V-ATPase B1 (Fig. 6b).

Discussion

$mCCD_{cl1}$ cells display bi-potential characteristics

At the population level our electrophysiological data show that $mCCD_{cl1}$ cells exhibited the expected transport characteristics of PCs, however the immunocytochemistry and RNA seq data suggest that results from the functional data cannot be extrapolated to the behaviour of individual cells.

Electrophysiological measurements from the parental $mCCD_{cl1}$ cell line gave results comparable to previous studies, including a 3.8 ± 0.2 fold change in I_{sc} following treatment with physiological concentration of aldosterone (33). This response was due to an increase in Na^+ reabsorption via ENaC, but the amiloride-insensitive I_{sc} demonstrates that a portion of the current is due to other electrogenic transport. Indeed application of $BaCl_2$ inhibited part of the remaining current (data not shown)., indicating K^+ secretion, likely via ROMK. Our data show that $mCCD_{cl1}$ cells, widely used as representative of PCs

for electrophysiology studies, expressed significant levels of IC markers. It is therefore possible that H^+ secretion via the apical V-ATPase in β-ICs may contribute to remainder of the amiloride-insensitive I_{sc}.

The presence of IC-specific transporter transcripts (for example the Na^+/H^+ exchanger (NHE3), NKCC1 (20), or H^+/K^+ ATPase (27)) suggests the possibility of IC-specific electroneutral ion transport. Such ion transport mechanisms would not be detectable in our electrophysiology measurements. The immunocytochemistry results showed that markers for both cell types were co-expressed in a significant portion (~42%) of the cell population and that the cell line is not simply a mixed population of differentiated PCs and ICs. The preponderance of cells expressing both PC and IC markers was also evident for the clonal sub-lines, thereby reinforcing the conclusion that this is an intrinsic property of $mCCD_{cl1}$ cells.

The ability of $mCCD_{cl1}$ cells to display differentiated characteristics of both PC and IC cells is reminiscent of the bi-potential of cell lines such as HepaRG (23). In addition to expressing genes characteristic of ICs and PCs our RNAseq data showed the expression of progenitor markers. The $mCCD_{cl1}$ cell line originated from a confluent primary culture of microdissected CCDs as a clone that spontaneously continued to divide in culture. Its capacity for generating both IC- and PC-like cells suggests that the immortalisation event(s) occurred in a bi-potential precursor cell resident in the CCD. The fact that the cell line was isolated from the adult tissue raises important questions regarding the potential for continuous physiological plasticity of the CCD *in vivo*. Further, the data provide evidence for the inter-relationship between these two anatomically co-localised cell types, however the details of this relationship cannot be determined from our present studies. Interestingly, the expression of p63 in particular hints at the pluripotent nature of the $mCCD_{cl1}$ cell line, and the potential for the line to be used as a model for differentiation and determination studies.

The immunocytochemistry results are consistent with the electrophysiological measurements

The presence of PC^+/IC^+ cells was transmitted through single cells of the parental $mCCD_{cl1}$ line to Ed1, Ed2, and Ed3, although in different proportions. The comparison of electrophysiological and immunocytochemistry data suggests that the composition of each cell line parallels their function. One might expect that a higher proportion of ENaC-expressing cells would result in higher Na^+ transport, however the presence of dual-staining cells complicates the picture. The parental cell line and Ed1 have a comparable proportion of cells expressing ENaC, but V-ATPase B1 is expressed in a greater number of Ed1 cells correlating with lower R_{te} and V_{te} values than in the parental line. A similar relationship between phenotype and function was observed for Ed2 and Ed3. The particularly small R_{te} measured for

Ed2 may be the result of a transitioning or undifferentiated state during which cells lose, or have not established, features such as tight junctions.

Transmission of both PC and IC characteristics to clonal sublines shows cell plasticity

Plasticity of the $mCCD_{cl1}$ cells was confirmed by the data obtained from the $mCCD_{cl1}$ sub-lines following single cell cloning. The nature of the PC^+/IC^+ cells could be described as bi-potential or displaying an 'immature' phenotype characteristic of precursor cells. There is evidence for cells transitioning from α to β-IC and from IC to PC *in vitro* (8, 34) but data on our clonal $mCCD_{cl1}$ sublines suggests a substantial degree of plasticity rather than uni-directional differentiation. The *in vivo* studies on Adam10 by Guo *et al* (14) confirms the existence of factors influencing the fate and ratio of collecting duct IC and PC cells through the Notch signalling pathway. They also showed that expression of Foxi1, which is important in the differentiation of IC cells, was altered, supporting the case for the maintenance of collecting duct cell plasticity *in vivo*. Ambiguous cell types ("hybrids") were observed by Wu *et al.* (37), where *Dot1l* deletion resulted in a ~15% rise in the number of ICs, seemingly derived from $Aqp2^+$ cells. In the same manner, ambiguous non-α non-β ICs have been observed and are speculated to be caught in a process of transition between α and β (27).

The RNA sequencing of $mCCD_{cl1}$ and the sublines confirmed the heterogenous characteristics of the clones by showing clear differences in expression between the lines. Whilst RNA expression is a good indicator of general transcriptional conditions in a cell population, it does not necessarily translate to protein concentration or function, but provides important evidence for the heterogeneity of the $mCCD_{cl1}$ cell population. These data suggest that studies using $mCCD_{cl1}$ cells should take account of the mixed nature of their phenotype and the influence that cell line composition may have, particularly when measuring the response of a population of cells as a whole, e.g. electrophysiological experiments. The precise culture conditions may affect cell phenotype to a greater or lesser extent and may, in part, explain variability between experiments.

The clonal cell lines maintain their characteristics through passaging

The argument that the $mCCD_{cl1}$ cell line represents a precursor-like state is supported by the fact that the individual sub-lines maintain a stable sub-line-specific distribution of cell types and electrophysiological properties for a minimum of four passages. Whether, after prolonged passaging, the sub-lines would revert to a common distribution of cell types and electrophysiology closer to that of the parental $mCCD_{cl1}$ cells, is unknown. The mechanism through which the sub-lines maintain their differences over passages is unclear but may reflect epigenetic differences, for example methylation status. It is clear that measurements of certain phenotypes, such as the electrophysiological characteristics reported here, are

based on the population of cells as a whole and yet the characteristics of individual cells making up the populations vary widely both within, and between, independent sub-lines derived originally from single cells. This raises interesting questions regarding the gene expression profile across a population of cells *versus* individual cells, and whether neighbouring cells, and the local environment, influence that expression.

It is impossible retrospectively to determine the nature of the single cells that gave rise to each sub-line, and they may have originated from any of the PC^+/IC^-, PC^-/IC^+, PC^+/IC^+, or PC^-/IC^- $mCCD_{cl1}$ cells from the parental population. However, following cloning they each gave rise to progeny that included all four phenotypic groups. We can speculate that all three sub-lines may have arisen from PC^+/IC^+ cells and that only these cells have the capacity to produce progeny of all four classes. From the present study there is no evidence to prove that this is the case and it does not alter the conclusions that $mCCD_{cl1}$ cells have bi-potential, display a spectrum of phenotypes from IC-like cells to PC-like cells, and that this potential can be transmitted vertically via a single cell. Prospective isolation of single cells of each class may enable further insights into the potential for differentiation of $mCCD_{cl1}$ cells, as would further investigation of the Notch pathway.

In vivo, ICs and PCs cells are clearly distinct. However, collecting ducts *in vivo* are in a highly regulated environment (6, 32), constantly under the influence of physiological factors that may be the key to keeping cells in a fully differentiated, more stable state. In this work, the correlation between the expression of V-ATPase A1 and the absence of acetylated α-tubulin could be used to identify cell types, but also suggests that the cells are structurally distinct, and that acetylation could be an important factor for the determination of CCD cell type.

Studies using gene knockout mice reported changes in the proportion of ICs and PCs or the existence of "hybrid" cells (37). Genetic models of kidney disease such as the syndrome of apparent mineralocorticoid excess (SAME) (18) may be informative for understanding the factors influencing collecting duct cell plasticity, through the observation of the CCD cellular response to induced transport modifications, for example the impaired Na^+ transport by ENaC in SAME. Whilst the consequences of common kidney diseases on sodium transport in the collecting duct are well documented, no specific data has been reported regarding the relative number of PCs and ICs, even though the ratio can affect renal fluid homeostasis. The observation of kidney tubules in real time under changing conditions such as drug treatment, acidosis, or sodium intake, could be a useful tool for recording functionally relevant shift between PCs and ICs *in vivo.*

Using $mCCD_{cl1}$ to develop kidney regeneration models

Since $mCCD_{cl1}$ cells have the capacity to form a resistive, polarized monolayer, their bi-potential precursor nature also makes the cell line an excellent model for studying remodelling, especially considering their expression of collecting duct precursor marker p63. Human adult kidney progenitor cells have been shown to be useful in the treatment of acute renal failure (29) and the characteristics of $mCCD_{cl1}$ cells make them potential candidates for the establishment of *in vitro* 3D models of the CCD.

Recent publication of single cell RNA-seq analysis of microdissected collecting ducts revealed a small fraction of cells, which clearly expressed both PC- and IC-specific transcripts (5). The potential for *in vivo* plasticity and adaptation of the collecting duct to physiological challenge or disease etiology through a shift in the PC/IC ratio may provide new leads for investigating factors that modify renal disease. As well as being used as a model of principal cells for electrophysiology studies, the $mCCD_{cl1}$ cell line has the potential to contribute to our understanding of cellular interconversion in the CCD and the factors influencing differentiation, renal injury and repair.

Acknowledgements

We gratefully acknowledge funding from BHF Centre for Research Excellence. Adrienne Assmus was the recipient of a 4-year BHF PhD studentship funded by the Centre of Research Excellence. We thank Bernard Rossier and Edith Hummler for kindly providing the $mCCD_{cl1}$ cells, and Johannes Loffing for the ENaC antibody. We thank Jamie Davies and Steve Morley for helpful comments on the manuscript. Finally we thank Charlotte Buckley for support with confocal microscopy in the CALM facility.

References

1. **Al-Awqati Q**. Cell biology of the intercalated cell in the kidney. *FEBS Lett* 587: 1911–1914, 2013.

2. **Andrews S**. FastQC A Quality Control tool for High Throughput Sequence Data [Online]. *http://www.bioinformatics.babraham.ac.uk/projects/fastqc/*: [date unknown]. http://www.bioinformatics.babraham.ac.uk/projects/fastqc/.

3. **Bolger AM**, **Lohse M**, **Usadel B**. Trimmomatic: a flexible trimmer for Illumina sequence data. *Bioinformatics* 30: 2114–2120, 2014.

4. **Boulkroun S**, **Ruffieux-Daidié D**, **Vitagliano J-J**, **Poirot O**, **Charles R-P**, **Lagnaz D**, **Firsov D**, **Kellenberger S**, **Staub O**. Vasopressin-inducible ubiquitin-specific protease 10 increases ENaC cell surface expression by deubiquitylating and stabilizing sorting nexin 3. *Am J Physiol Renal Physiol* 295: F889-900, 2008.

5. **Chen L**, **Lee JW**, **Chou C-L**, **Nair A V.**, **Battistone MA**, **Păunescu TG**, **Merkulova M**, **Breton S**, **Verlander JW**, **Wall SM**, **Brown D**, **Burg MB**, **Knepper MA**. Transcriptomes of major renal collecting duct cell types in mouse identified by single-cell RNA-seq. *Proc. Natl. Acad. Sci.* (2017). doi: 10.1073/pnas.1710964114.

6. **Dantzler WH**. Regulation of renal proximal and distal tubule transport: sodium, chloride and organic anions. *Comp Biochem Physiol Part A Mol Integr Physiol* 136: 453–478, 2003.

7. **El-dahr SS**, **Li Y**, **Liu J**, **Gutierrez E**, **Hering-smith KS**, **Signoretti S**, **Pignon J**, **Sinha S**, **Saifudeen Z**. p63 + ureteric bud tip cells are progenitors of intercalated cells. 2: 1–9, 2017.

8. **Fejes-Tóth G**, **Náray-Fejes-Tóth A**. Differentiation of renal beta-intercalated cells to alpha-intercalated and principal cells in culture. *Proc Natl Acad Sci U S A* 89: 5487–91, 1992.

9. **Fodstad H**, **Gonzalez-Rodriguez E**, **Bron S**, **Gaeggeler H**, **Guisan B**, **Rossier BC**, **Horisberger J-D**. Effects of mineralocorticoid and K+ concentration on K+ secretion and ROMK channel expression in a mouse cortical collecting duct cell line. *Am J Physiol Renal Physiol* 296: F966–F975, 2009.

10. **Ford P**, **Rivarola V**, **Chara O**, **Blot-Chabaud M**, **Cluzeaud F**, **Farman N**, **Parisi M**, **Capurro C**. Volume regulation in cortical collecting duct cells: role of AQP2. *Biol Cell* 97: 687–697, 2005.

11. **Gaeggeler H-P**, **Gonzalez-Rodriguez E**, **Jaeger NF**, **Loffing-Cueni D**, **Norregaard R**, **Loffing J**, **Horisberger J-D**, **Rossier BC**. Mineralocorticoid versus glucocorticoid receptor occupancy mediating aldosterone-stimulated sodium transport in a novel renal cell line. *J Am Soc Nephrol* 16: 878–891, 2005.

12. **Gao X**, **Eladari D**, **Leviel F**, **Tew BY**, **Miro-Julia C**, **Cheema FH**, **Miller L**, **Nelson R**, **Paunescu TG**, **McKee M**, **Brown D**, **Al-Awqati Q**. Deletion of hensin/DMBT1 blocks conversion of - to -intercalated cells and induces distal renal tubular acidosis. *Proc Natl Acad Sci* 107: 21872–21877, 2010.

13. **Gueutin V**, **Vallet M**, **Jayat M**, **Peti-peterdi J**, **Cornière N**, **Leviel F**, **Sohet F**, **Wagner CA**, **Eladari D**, **Chambrey R**. Renal β -intercalated cells maintain body fluid and electrolyte balance. 123: 4219–4231, 2013.

14. **Guo Q**, **Wang Y**, **Tripathi P**, **Manda KR**, **Mukherjee M**, **Chaklader M**, **Austin PF**, **Surendran K**, **Chen F**. Adam10 Mediates the Choice between Principal Cells and Intercalated Cells in the Kidney. *J. Am. Soc. Nephrol.* (2014). doi: 10.1681/ASN.2013070764.

15. **Jeong H**, **Jeon US**, **Koo B**, **Kim W**, **Im S**, **Shin J**, **Cho Y**, **Kim J**, **Kong Y**. Inactivation of Notch signaling in the renal collecting duct causes nephrogenic diabetes insipidus in mice. 119, 2009.

16. **Kim D**, **Langmead B**, **Salzberg SL**. HISAT: A fast spliced aligner with low memory requirements. *Nat Methods* 12: 357–360, 2015.

17. **Kim J**, **Kim YH**, **Cha JH**, **Tisher CC**, **Madsen KM**. Intercalated cell subtypes in connecting tubule and cortical collecting duct of rat and mouse. *J Am Soc Nephrol* 10: 1–12, 1999.

18. **Kotelevtsev Y**, **Seckl JR**, **Mullins JJ**. 11β-Hydroxysteroid dehydrogenases: key modulators of glucocorticoid action in vivo [Online]. *Curr Opin Endocrinol Diabetes Obes* 6, 1999. http://journals.lww.com/co-endocrinology/Fulltext/1999/06000/11__Hydroxysteroid_dehydrogenases__key_modulators.4.aspx.

19. **Langworthy M**, **Zhou B**, **de Caestecker M**, **Moeckel G**, **Baldwin HS**. NFATc1 identifies a population of proximal tubule cell progenitors. *J Am Soc Nephrol* 20: 311–321, 2009.

20. **Leviel F**, **Hübner CA**, **Houillier P**, **Morla L**, **Moghrabi S El**, **Brideau G**, **Hatim H**, **Parker MD**, **Kurth I**, **Kougioumtzes A**, **Sinning A**, **Pech V**, **Riemondy KA**, **Miller RL**, **Hummler E**, **Shull GE**, **Aronson PS**, **Doucet A**, **Wall SM**, **Chambrey R**, **Eladari D**. The Na + -dependent chloride-bicarbonate exchanger SLC4A8 mediates an electroneutral Na + reabsorption process in the renal cortical collecting ducts of mice. 120: 1627–1635, 2010.

21. **Mansley MK**, **Neuhuber W**, **Korbmacher C**, **Bertog M**. Norepinephrine stimulates the epithelial Na^+ channel in cortical collecting duct cells via α_2 -adrenoceptors. *Am J Physiol - Ren Physiol* 308: F450–F458, 2015.

22. **Mironova E**, **Peti-Peterdi J**, **Bugaj V**, **Stockand JD**. Diminished paracrine regulation of the epithelial Na+ channel by purinergic signaling in mice lacking connexin 30. *J Biol Chem* 286: 1054–1060, 2011.

23. **Parent R**, **Marion MJ**, **Furio L**, **Trépo C**, **Petit MA**. Origin and Characterization of a Human Bipotent Liver Progenitor Cell Line. *Gastroenterology* 126: 1147–1156, 2004.

24. **Patro R**, **Duggal G**, **Kingsford C**. Salmon: Accurate, Versatile and Ultrafast Quantification from RNA-seq Data using Lightweight-Alignment [Online]. *bioRxiv*. http://biorxiv.org/content/early/2015/06/27/021592.abstract.

25. **Robinson MD**, **McCarthy DJ**, **Smyth GK**. edgeR: a Bioconductor package for differential expression analysis of digital gene expression data. *Bioinformatics* 26: 139–140, 2010.

26. **Robinson MD**, **Oshlack A**. A scaling normalization method for differential expression analysis of RNA-seq data. *Genome Biol* 11: R25, 2010.

27. **Roy A**, **Al-Bataineh MM**, **Pastor-Soler NM**. Collecting duct intercalated cell function and regulation. *Clin J Am Soc Nephrol* 10: 305–324, 2015.

28. **Ryan JA**. Cell Cloning by Serial Dilution in 96 Well Plates Protocol. *Life Sci* : 10–12, 2008.

29. **Sagrinati C**. Isolation and Characterization of Multipotent Progenitor Cells from the Bowman's Capsule of Adult Human Kidneys. *J Am Soc Nephrol* 17: 2443–2456, 2006.

30. **De Seigneux S**, **Leroy V**, **Ghzili H**, **Rousselot M**, **Nielsen S**, **Rossier BC**, **Martin PY**, **Féraille E**. NF-κB inhibits sodium transport via down-regulation of SGK1 in renal collecting duct principal cells. *J Biol Chem* 283: 25671–25681, 2008.

31. **Soneson C**, **Love MI**, **Robinson MD**. Differential analyses for RNA-seq: transcript-level estimates improve gene-level inferences [version 1; referees: 2 approved]. *F1000Research* 4, 2015.

32. **Staruschenko A**. Regulation of transport in the connecting tubule and cortical collecting duct. (2013). doi: 10.1002/cphy.c110052.Regulation.

33. **Svenningsen P**, **Burford JL**, **Peti-Peterdi J**. ATP releasing connexin 30 hemichannels mediate flow-induced calcium signaling in the collecting duct. *Front Physiol* 4: 292, 2013.

34. **Trepiccione F**, **Capasso G**, **Nielsen S**, **Christensen BM**. Evaluation of cellular plasticity in the collecting duct during recovery from lithium-induced nephrogenic diabetes insipidus. *Am J Physiol Renal Physiol* 305: F919-29, 2013.

35. **Wang L**, **Wang S**, **Li W**. RSeQC: quality control of RNA-seq experiments. *Bioinformatics* 28: 2184–2185, 2012.

36. **Werth M**, **Schmidt-Ott KM**, **Leete T**, **Qiu A**, **Hinze C**, **Viltard M**, **Paragas N**, **Shawber CJ**, **Yu W**, **Lee P**, **Chen X**, **Sarkar A**, **Mu W**, **Rittenberg A**, **Lin CS**, **Kitajewski J**, **Al-Awqati Q**, **Barasch J**. Transcription factor TFCP2l1 patterns cells in the mouse kidney collecting ducts. *Elife* 6: 1–24, 2017.

37. **Wu H**, **Chen L**, **Zhou Q**, **Zhang X**, **Berger S**, **Bi J**, **Lewis DE**, **Xia Y**, **Zhang W**. Aqp2-Expressing Cells Give Rise to Renal Intercalated Cells. *J Am Soc Nephrol* 24: 243–252, 2013.

38. **Xiao Z**, **Chen L**, **Zhou Q**, **Zhang W**. Dot1l de fi ciency leads to increased intercalated cells and upregulation of V-ATPase B1 in mice. *Exp Cell Res* 344: 167–175, 2016.

Figure legends

Figure 1. *$mCCD_{cl1}$ cells express both PC and IC markers.*

(a) Immunostaining of $mCCD_{cl1}$ cells cultured on filters using anti-Aqp2 (green) and anti-Cx30 (red) antibodies as PC and IC markers respectively. Scale bar 20µm (b) Immunostaining of $mCCD_{cl1}$ cells using anti-Aqp2 (green) and anti-V-ATPase B1 (red) antibodies PC and IC markers respectively. Scale bar 20 µm (c) Immunostaining of $mCCD_{cl1}$ cells using anti-α-ENaC (red) and anti-V-ATPase A1 (green) antibodies. Scale bar 20µm (d) Higher magnification of Aqp2 (green) and Cx30 (red) immunostaining of $mCCD_{cl1}$ cells. Scale bar 10µm. In all the merged pictures, DAPI staining of cell nuclei. (e) Confocal image and orthogonal projections (right and bottom) of $mCCD_{cl1}$ cultured on filter with α-ENaC immunostaining in red over the greyscale autofluorescence of the cells. The orthogonal planes correspond to cells along the crosshairs (red lines). White scale bar is 20µm.

Figure 2. *Acetylated α-tubulin staining detects primary cilia, but also tubular cytoskeleton of PC-like cells.*

(a) Immunostaining of $mCCD_{cl1}$ using anti acetylated α-tubulin (green), anti-V-ATPase A1 (light blue) and anti-α-ENaC (red) antibodies. DAPI staining of cell nuclei in the merged picture. The magnified area highlights a region of interest where the inverse correlation between V-ATPase A1 and acetylated α-tubulin, quantified in (c), is particularly notable. Scale bar 20µm. (b) Immunostaining of acetylated α-tubulin and α-ENaC, focused on the apical membrane of $mCCD_{cl1}$ cells to detect primary cilia, shown by the white arrows. Scale bar 20µm. (c) Mean grey value of cells showing different expression levels of V-ATPase A1 and acetylated α-tubulin. Left panel: paired t-test, orange for high levels of V-ATPase A1 , blue for low levels. Right panel: data ordered by increasing V-ATPase A1 mean grey value. Red dotted line at 5% indicates the limit chosen to define high and low levels of V-ATPase A1.

Figure 3. *Both PC and IC phenotypes are transmitted to the clonal cell lines, in different proportions.*

(a) Representative images of $mCCD_{cl1}$, Ed1, Ed2, and Ed3 stained with anti-Aqp2 (green) and anti-V-ATPase B1 (red) antibodies. DAPI staining of cell nuclei is shown in the merged pictures. Magnification x40. Scale bar 20µm. (b) Quantification of the proportion of cells (%) staining for Aqp2 only, V-ATPase B1 only, both, or neither in $mCCD_{cl1}$, Ed1, Ed2, and Ed3. (c) RT-PCR results of Aqp2 and Cx30 in the $mCCD_{cl1}$ parental (Par), and clonal lines Ed1, Ed2, and Ed3. C1, C2 are negative controls. (d)

Representative images of $mCCD_{cl1}$, Ed1, Ed2, and Ed3 cells stained with anti-α-ENaC (red), and DAPI staining of cell nuclei. Magnification x40. Scale bar 20μm. (e) Mean grey value per cell line showing different expression levels of α-ENaC in $mCCD_{cl1}$, Ed1, Ed2, and Ed3 cells.

Figure 4. *Parental $mCCD_{cl1}$ and subline cells have different electrophysiological properties*

(a) Transepithelial voltage (V_{te}) measured across monolayers of $mCCD_{cl1}$, Ed1, Ed2, and Ed3 cells grown on Snapwells filters, between day 3 and 10 after seeding. (b) Transepithelial resistance (R_{te}) measured across monolayers of $mCCD_{cl1}$, Ed1, Ed2, and Ed3 cells. (c) I_{sc} was calculated using Ohm's law. Values are shown as mean ± SEM (n=4). (d) Effects on baseline I_{sc} of aldosterone (3nM) and amiloride (10μM, apical bath) added at t=0 and t=120min respectively. Values are shown as mean ± SEM (n=4).

Figure 5. *Transcriptomes of $mCCD_{cl1}$, Ed1, Ed2, and Ed3 are distinct.*

(a) Principal component analysis results displayed in a 3D matrix. The axes are the first three principal components (PC1, PC2, and PC3), with the corresponding percentage of total variability they represent in the dataset. Each geometric figure represents one sample, with the repeats (n=3) given the same shape. (b) Clustering dendrogram analysis, based on the top 1000 genes with the most important variance between the samples. The height of the bars is a measure of dissimilarity between samples. The repeats of the same cell line are in the same shape.

Figure 6. *$mCCD_{cl1}$, Ed1, Ed2, and Ed3 express collecting duct progenitor markers p63 and ΔNp63*

(a) Representative images of $mCCD_{cl1}$, Ed1, Ed2 and Ed3 stained with anti-p63 (green) and anti-ΔNp3 (red) antibodies. DAPI staining in blue in the merged picture. Magnification x40. Scale bar 20μm. (b) Representative images of mCCDcl1 stained with anti-V-ATPase B1 (red) and anti-p63 (green) antibodies. DAPI staining in blue in the merged picture. Magnification x60. Scale bar 15μm.

Tables

Table 1. Primers used for RT-PCR of Cx30 and Aqp2

	Gene	Genbank ID	Forward primer	Reverse primer	Product size, bp
Aquaporin 2	Aqp2	NC_000081.6	5'-atgtgggaactccggtccata-3'	5'-acggcaatctggagcacag-3'	137
Connexin 30	Gjb6	NC_000080.6	5'-accagcatagggaaggtgtg-3'	5'-tgcagagtgttgcagacaaag-3'	119

Table 2. Electrophysiological measurements for the parental mCCDcl1 cell line and the clonal sublines Ed1, Ed2 and Ed3, and calculated Isc fold change after aldosterone treatment and Isc blocked from amiloride treatment.

		Baseline ± SD	Aldosterone 3h ± SD	Amiloride 10min ± SD	Isc Fold change, aldosterone treatment ± SD	% of Isc blocked by amiloride ± SD
$mCCD_{cl1}$	I_{sc} ($\mu A/cm^2$)	-9.0 ± 1.0	-34.0 ± 1.2	-1.6 ± 0.7	3.8 ± 0.3	82.1 ± 8.2
	R_{te} ($k\Omega \cdot cm^2$)	1.6 ± 0.1	1.0 ± 0.1	2.1 ± 0.1		
	V_{te} (mV)	-14.7 ± 1.5	-37.6 ± 0.8	-3.5 ± 1.6		
Ed1	I_{sc} ($\mu A/cm^2$)	-11.4 ± 0.9	-22.6 ± 0.7	-2.1 ± 0.8	2.1 ± 0.2	81.8 ± 7.0
	R_{te} ($k\Omega \cdot cm^2$)	0.8 ± 0.1	0.7 ± 0.0	1.0 ± 0.1		
	V_{te} (mV)	-8.7 ± 1.2	-16.0 ± 0.8	-2.1 ± 0.8		
Ed2	I_{sc} ($\mu A/cm^2$)	-1.4 ± 0.4	-4.1 ± 0.2	-0.9 ± 0.3	3.9 ± 1.2	36.4 ± 7.0
	R_{te} ($k\Omega \cdot cm^2$)	0.8 ± 0.1	0.8 ± 0.1	1.0 ± 0.1		
	V_{te} (mV)	-1.2 ± 0.4	-3.4 ± 0.4	-0.9 ± 0.3		
Ed3	I_{sc} ($\mu A/cm^2$)	-12.8 ± 0.8	-27.1 ± 0.8	-1.4 ± 0.4	2.1 ± 0.2	88.4 ± 3.1
	R_{te} ($k\Omega \cdot cm^2$)	2.6 ± 0.2	-2.0 ± 0.1	4.1 ± 0.3		
	V_{te} (mV)	-33.1 ± 3.8	-54.0 ± 1.9	-6.3 ± 2.1		

Table 3. Summary of the cell characteristics based on the immunocytochemistry data

	PC^+/IC^-	**PC^-/IC^+**	**PC^+/IC^+**	**PC^-/IC^-**
Aqp2 staining	yes	no	yes	no
V-ATPase B1 staining	no	yes	yes	no
Acetylated α-tubulin staining	high	low or absent	low or absent	low or absent

Table 4. Top twenty differentially expressed transcripts between parental cell line and each clonal cell line, ordered by decreasing fold change.

Parental vs Ed1				Parental vs Ed2			
Gene name	Ed1 (cpm)	Parental (cpm)	Fold change	Gene name	Ed2 (cpm)	Parental (cpm)	Fold change
Gm20388	0.12	94.13	784.42	*Pdlim1*	0.16	6.52	40.73
Ldoc1l	0.12	6.79	56.58	*Crip1*	0.29	9.4	32.4
Ap1m2	0.37	15.47	41.82	*Kcnj10*	0.27	8.01	29.68
Ndn	0.19	5.5	29.48	*Rhcg*	1.99	56.87	28.53
Gm13212	0.61	14.7	24.23	*Sirpa*	0.14	3.67	26.21
Egln3	4.81	109.13	22.69	*Bsnd*	2	49.82	24.95
Eya4	0.14	2.31	16.5	*Nid2*	0.2	4.24	21.56
Gm13157	1.63	25.53	15.69	*Gm20388*	4.62	94.13	20.39
Tmem22a	0.21	3.22	15.56	*Arrdc4*	0.19	3.24	16.78
Lhx1	0.23	3.38	14.5	*Kcnj1*	1.63	26.93	16.55
Igfbp5	53.05	4.61	-11.5	*Tmem25c*	1.84	0.26	-7.09
Ccl17	8.09	0.7	-11.5	*Egr2*	11.26	1.26	-8.91
Chst11	3.43	0.29	-11.83	*Pga5*	3.78	0.41	-9.3
Gm26822	669.62	54.73	-12.24	*Nr4a3*	3.43	0.36	-9.45
Gm15039	7.28	0.44	-16.41	*Prss56*	1.42	0.15	-9.49
Peg3	684.3	38.41	-17.82	*Areg*	12.01	1.15	-10.44
Nt5e	16.32	0.8	-20.31	*Angpt2*	66.68	5.03	-13.25
Mgp	6.51	0.27	-23.82	*Gm9755*	4.47	0.28	-15.96
Vgf	12.77	0.53	-24.1	*Vgf*	17.4	0.53	-32.84
Arvcf	10.31	0.12	-85.94	*Arvcf*	9.96	0.12	-82.97

Parental vs Ed3

Gene name	Ed1 (cpm)	Parental (cpm)	Fold change
Gm10443	0.12	5.22	43.47
Gm20388	2.34	94.13	40.17
Gm45140	0.5	15.36	30.93
Atp6v1b1	0.56	10.89	19.57
Kcnj1	1.46	26.93	18.44
Pcdh17	2	34.27	17.17
Naip6	0.81	12.43	15.41
Clcnkb	0.22	3.1	13.87
Eva1b	0.18	2.28	12.45
Fam84a	0.12	1.43	11.92
Loxl1	2.83	0.49	-5.78
Gm26778	2.94	0.45	-6.59
Mmp24	7.31	1.1	-6.67
Dmrtc1a	1.51	0.2	-7.44
Tmem254c	1.94	0.26	-7.46
Kctd12	84.5	11.16	-7.57
Gm11749	1.7	0.18	-9.29

Sytl2	60.2	6.37	-9.45
Trps1	6.51	0.69	-9.48
Arvcf	8.15	0.12	-67.89

675

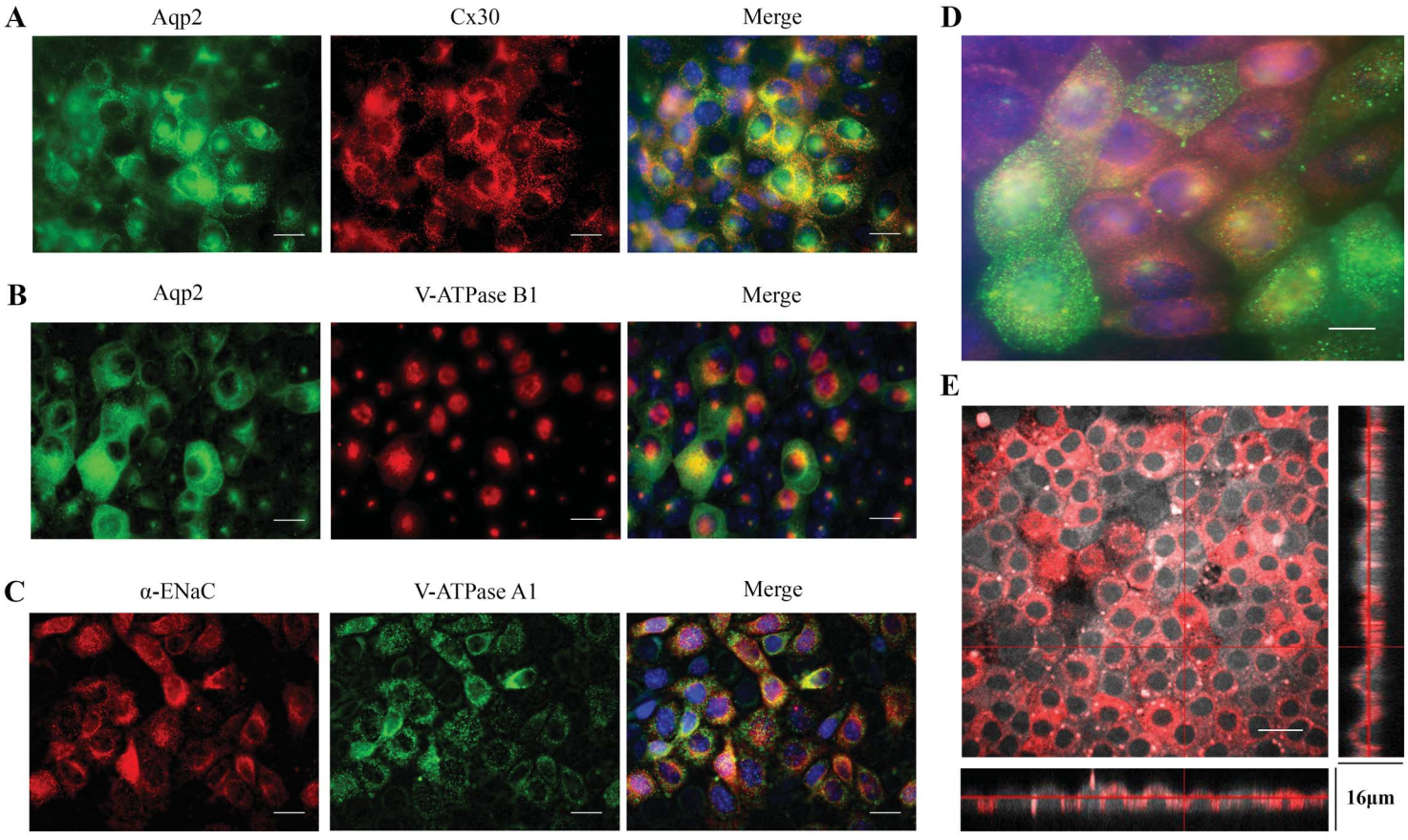
A
Aqp2
Cx30
Merge
B
Aqp2
V-ATPase B1
Merge
C
α-ENaC
V-ATPase A1
Merge
D
E
16μm

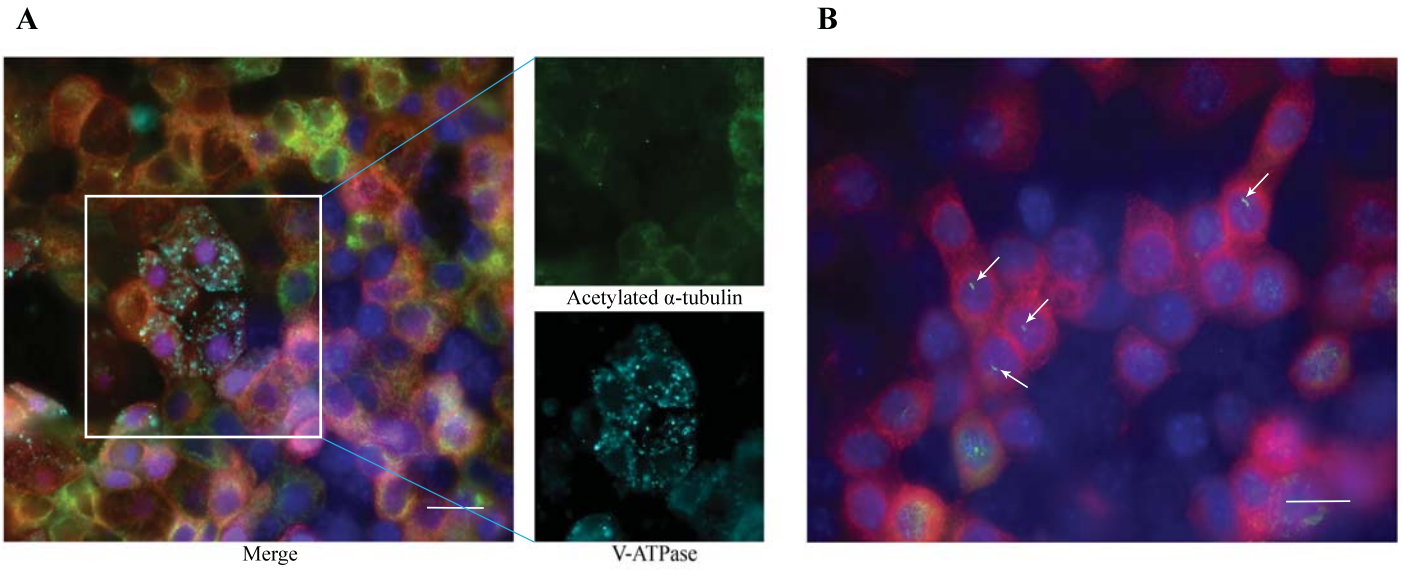
A
B
Acetylated α-tubulin
Merge
V-ATPase

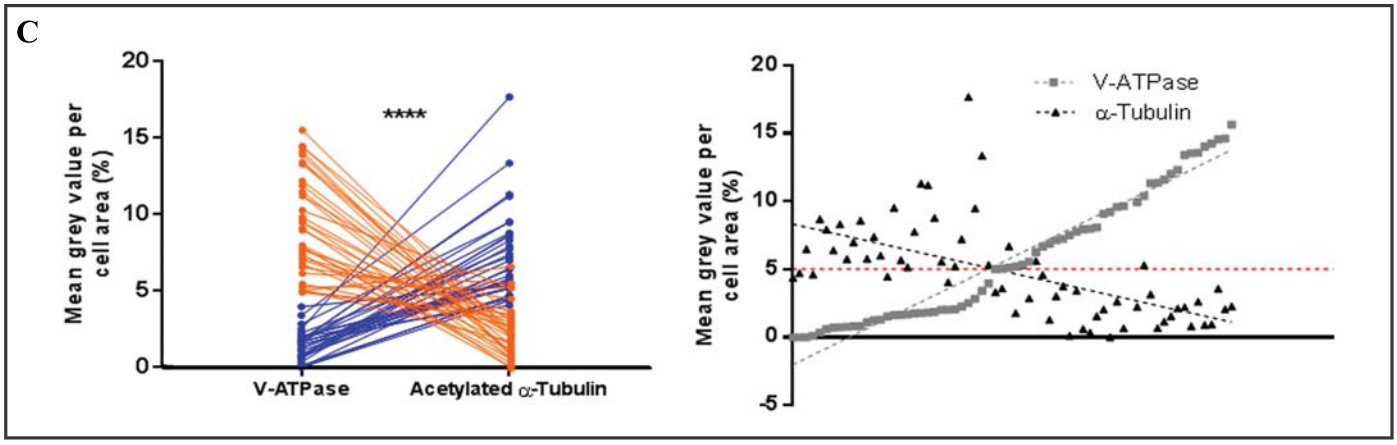
C
Mean grey value per cell area (%)
20
15
10
5
0
****
V-ATPase
Acetylated α-Tubulin
Mean grey value per cell area (%)
20
15
10
5
0
-5
V-ATPase
α-Tubulin

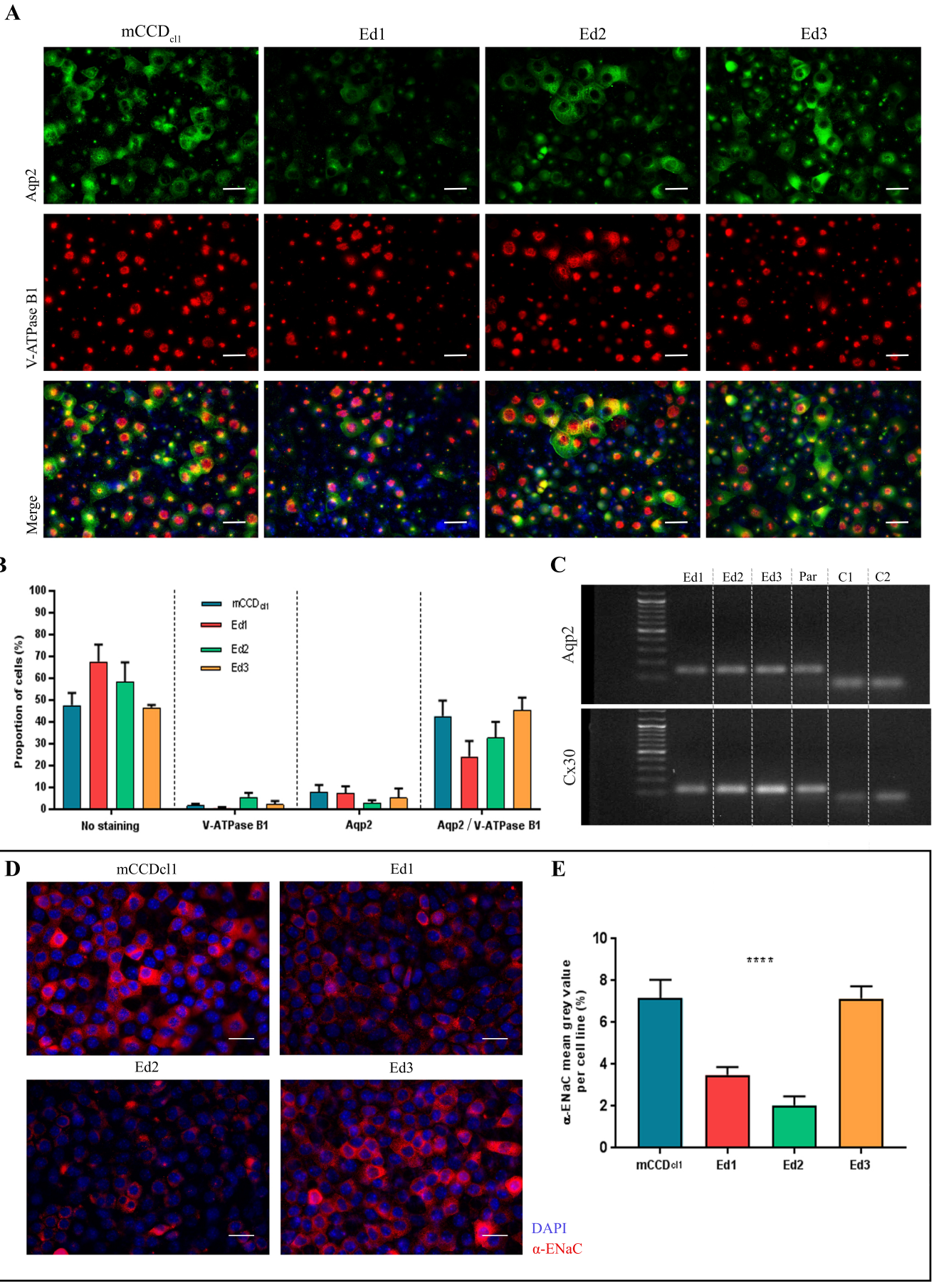
A
mCCDcl1
Ed1
Ed2
Ed3
Aqp2
V-ATPase B1
Merge
B
Proportion of cells (%)
mCCDcl1
Ed1
Ed2
Ed3
No staining
V-ATPase B1
Aqp2
Aqp2 / V-ATPase B1
C
Ed1
Ed2
Ed3
Par
C1
C2
Aqp2
Cx30
D
mCCDcl1
Ed1
Ed2
Ed3
DAPI
α-ENaC
E
α-ENaC mean grey value per cell line (%)
****
mCCDcl1
Ed1
Ed2
Ed3

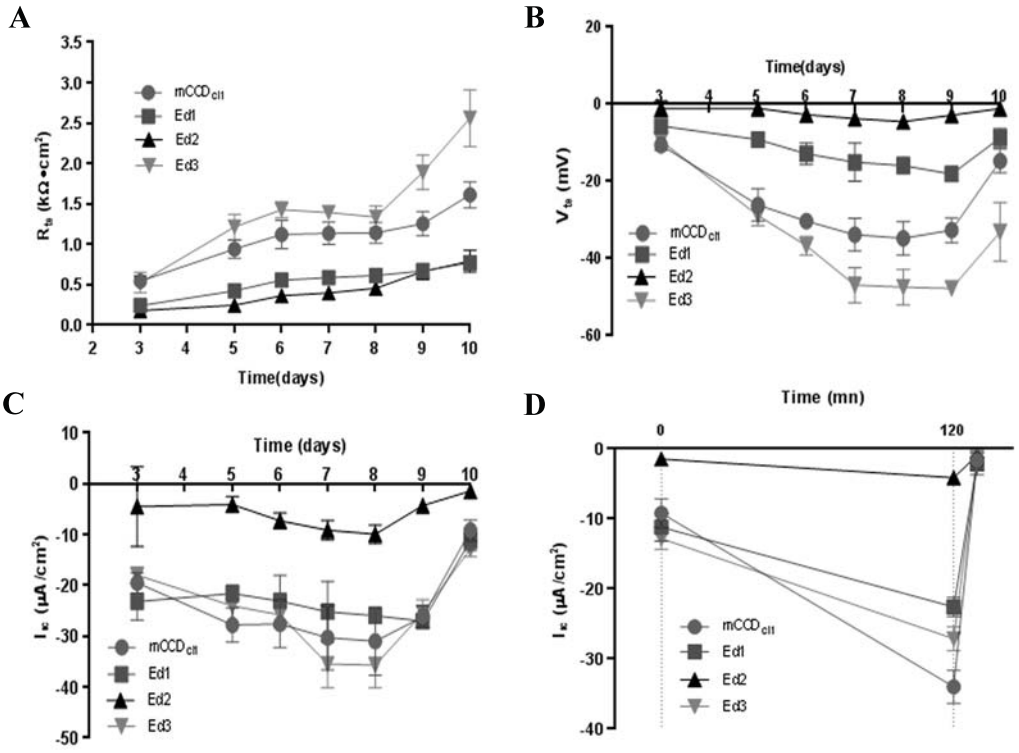
A
B
C
D
Time(days)
Time (mn)
mCCD cl1
Ed1
Ed2
Ed3

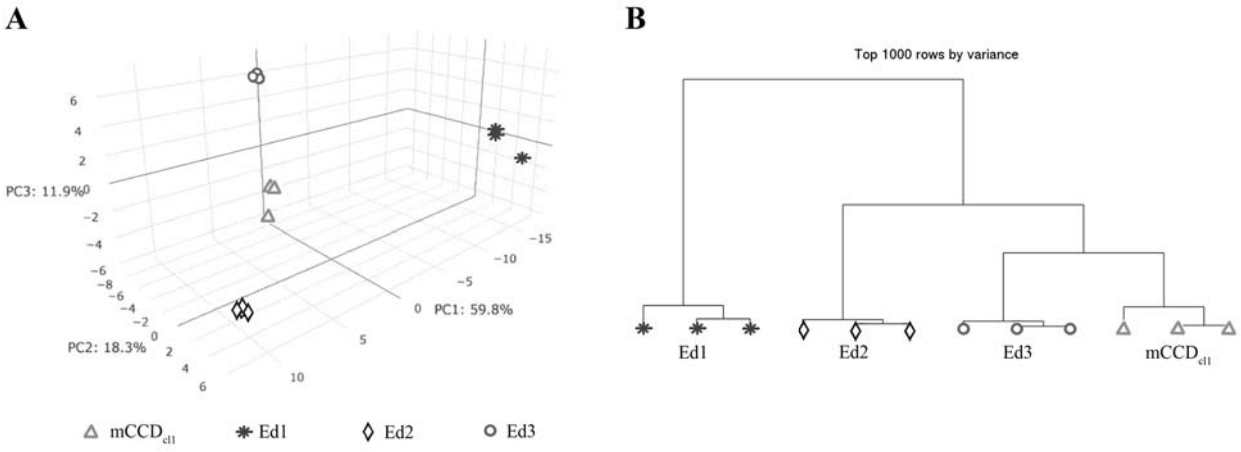
A
PC3: 11.9%
PC2: 18.3%
PC1: 59.8%
mCCD$_{cl1}$
Ed1
Ed2
Ed3
B
Top 1000 rows by variance
Ed1
Ed2
Ed3
mCCD$_{cl1}$

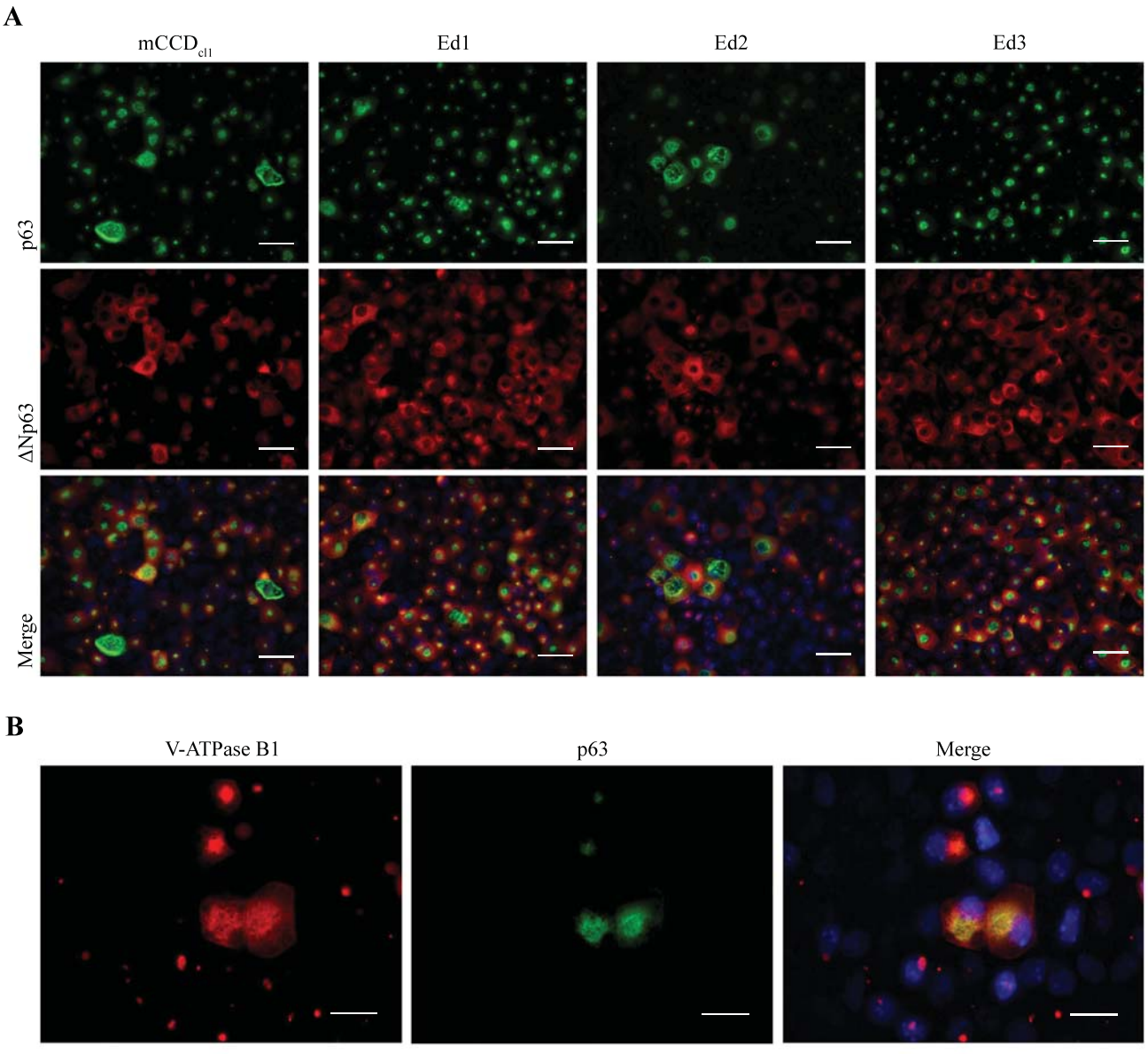
A
mCCD$_{cl1}$
Ed1
Ed2
Ed3
p63
ΔNp63
Merge
B
V-ATPase B1
p63
Merge